Theor Chem Acc (2012) 131:1147
DOI 10.1007/s00214-012-1147-5

REGULAR ARTICLE

First-principles simulations of the ^{27}Al and ^{17}O solid-state NMR spectra of the $CaAl_2Si_3O_{10}$ glass

Alfonso Pedone · Elisa Gambuzzi · Gianluca Malavasi · Maria Cristina Menziani

Received: 23 June 2011 / Accepted: 2 September 2011 / Published online: 15 February 2012

Abstract The local and medium-range structure of the $20CaO{\cdot}20Al_2O_3{\cdot}60SiO_2$ glass generated by classical molecular dynamics simulations has been compared to NMR experiments by computing the ^{27}Al and ^{17}O NMR parameters and NMR spectra from first-principles simulations. The calculation of the NMR parameters (chemical shielding and quadrupolar parameters), which are then used to simulate solid-state MAS and 3QMAS NMR spectra, is achieved by the gauge including projector augmented-wave and the projector augmented-wave methods on the DFT-PBE relaxed structure. The NMR spectra calculated with the present approach are found to be in excellent agreement with the experimental data, providing an unambiguous view of the local and medium-range structure of aluminosilicate glasses.

Keywords First-principles simulations · NMR spectra · Silicate glass · 3D structure

1 Introduction

In the recent decades, silica-based glasses have emerged as fundamental materials for new technological applications regarding data processing and transmission (optical fiber amplifiers, semiconductor devices), nuclear waste confinement and biomaterials (bioactive glasses).

To rationalize and predict the macroscopic thermodynamic and transport properties of such materials, a microscopic understanding of their structure and dynamics is required [1, 2].

Solid-state NMR spectroscopy has proven to be a very useful and versatile technique for studying the structure and the dynamics of non-crystalline materials such as oxide glasses and melts since long time [1, 3]. The effectiveness of NMR spectroscopy relies on the strong correlation between NMR observables (chemical shifts, quadrupolar parameters, couplings between nuclides) and the short- and medium-range structure of spin active nuclei constituting the glass [1].

The directional character of many NMR interactions coupled with the rigidity of structural units in non-crystalline solids results in heavily broad lineshapes, which can be envisioned as being composed of a series of narrow lines, each coming from a different crystallite orientation with respect to the external magnetic field. For this reason, more effort over the last 40 years has been devoted to the development of ways to average the anisotropic broadening in an artificial way, either by manipulating the spins or by manipulating the sample.

Initial experiments were focused on magic angle spinning [4–7] (MAS), which has been extensively applied to cancel out the effect of dipolar and chemical shift anisotropies of spin ½ nuclei (such as ^{29}Si) in silica-based glasses. This technique fails to remove the second-order quadrupolar effects present for nuclei with half-integer nuclear spin (so-called half-integer quadrupolar nuclei, here ^{17}O (I = 5/2), ^{43}Ca (I = 7/2), ^{27}Al (I = 5/2)); therefore, new techniques such as dynamic angle spinning (DAS), double rotation (DOR), or multiquantum magic angle spinning (MQMAS) have been developed [8, 9].

Dedicated to Professor Vincenzo Barone and published as part of the special collection of articles celebrating his 60th birthday.

A. Pedone · E. Gambuzzi · G. Malavasi · M. C. Menziani (✉)
Dipartimento di Chimica, Università degli Studi di Modena e Reggio Emilia, Via Campi 183, 41125 Modena, Italy
e-mail: menziani@unimo.it

Although experiments of this kind allow a high resolution in crystalline materials, the disorder and variety of structural units (different coordination numbers and Qn distributions, where n is the number of bridging oxygens (BO) around a network former species T = Si/Al) present in glasses make the interpretation difficult.

Traditionally, the interpretation of spectra of amorphous materials of unknown structure has been generally based on empirical correlations derived from the study of crystalline materials with known structure. However, there is still a need for much more work of this type, to establish and refine correlations between NMR observables and structural parameters.

Theoretical calculations of NMR parameters and structural correlations have been very helpful in interpreting spectra of glasses [10–12]. Since NMR interactions are essentially dependent upon local properties and are dominated by bonding in the first few coordination spheres, most of the theoretical investigations were performed on small molecular clusters using atomic orbital basis sets [13, 14]. The accuracy of this approach is limited by the choice of parameters such as the size of the cluster, the termination of the dangling bonds produced on cutting the cluster from the infinite solid (for covalent solids), or the treatment of the electrostatic interactions. Moreover, in the special case of amorphous materials, the cluster approach does not account for the correlations between structural factors that exist in solids and disorder in glasses.

These problems have been overcome with the introduction of effective methods specially devised to calculate NMR parameters in extended systems described within periodic boundary conditions, plane wave basis sets and density functional theory [15, 16].

The chemical shifts and the electric field gradients can be obtained from first principle with the gauge including projector augmented-wave (GIPAW) and the projector augmented-wave (PAW) methods, respectively [15, 16]. These methods are able to deal with large systems (up to hundreds of atoms), and exhibit an outstanding accuracy, as demonstrated recently for various crystalline and amorphous crystalline solids [12, 16–19].

Recently, Pedone et al. [10, 11] have reproduced, for the first time, the MAS and 3QMAS NMR solid-state spectra of spin active nuclei (^{29}Si, ^{31}P, ^{43}Ca,^{17}O and ^{23}Na) for the $CaSiO_3$ and the $46.1SiO_2{\cdot}24.4Na_2O{\cdot}26.9CaO{\cdot}2.6P_2O_5$ (45S5) glasses using a combined classical molecular dynamics simulations for generating the glass structure and periodic DFT calculations to obtain NMR parameters. The latter were introduced in spin-effective Hamiltonian encoded into a home-made package named fpNMR to simulate the spectra [10].

This integrated computational approach proved to be very useful to interpret the experimental spectra of the aforementioned nuclei and to gain new insights into the atomistic structure of very complex oxide glasses such as calcium-silicate and phospho-silicate glasses containing sodium and calcium ions.

The aim of the present work is to describe and apply the integrated computational procedure developed in the recent years to the simulation of the ^{27}Al, ^{17}O MAS and MQMAS solid-state spectra of a calcium aluminum–silicate (CAS) glass of composition $20CaO{\cdot}20Al_2O_3{\cdot}60SiO_2$, in order to obtain an unambiguous view of its local and medium-range structure around aluminum and oxygen atoms.

2 Computational details

2.1 Glass generation

Two three-dimensional structures of a calcium aluminosilicate glass with composition $20CaO{\cdot}20Al_2O_3{\cdot}60SiO_2$ were generated by means of classical molecular dynamics simulations. The shell model approach [20, 21] is used in the potential to include polarization effects, by taking into account the large polarizability of oxygen ions. In this model, the total charge Z of the oxygen ions is split between a core (of charge Z + Y) and a massless shell (of charge –Y), which are coupled by a harmonic spring. Besides the damped harmonic interaction with the corresponding core, the oxygen shells interact with each other and with Si, Al and Ca cations through a short-range Buckingham term, whereas coulombic forces act between all species which bear full formal charges. Three-body screened harmonic potentials are used to control the intra-tetrahedral O–Si–O and O–Al–O angles during dynamics. The expression for the complete potential model is therefore

$$U_{ij}(r_{ij}) = \frac{q_i q_j}{r_{ij}} + A_{ij} e^{-\left(\frac{r_{ij}}{\rho_{ij}}\right)} - \frac{C_{ij}}{r_{ij}^6} \quad (1)$$

$$U_{ijk}(\theta_{ijk}) = \frac{1}{2} k_b (\theta_{ijk} - \theta_0)^2 \exp\left\{ -\left(\frac{r_{ij}}{\rho_{ijk}} + \frac{r_{jk}}{\rho_{ijk}} \right) \right\} \quad (2)$$

$$U_{\text{core-shell}}(r_{\text{core-shell}}) = \frac{1}{2} k_s (r_{\text{core-shell}})^2 \quad (3)$$

The complete potential model and the parameters [22] used are reported in Table 1. The leap-frog algorithm encoded in the DL_POLY package [23] has been used to integrate the equation of motions with a time step of 0.2 fs small enough to control the high-frequency motion of the core–shell spring during MD simulations [24].

The initial configurations were generated by placing randomly 250 atoms in a cubic box of 14.98 Å accordingly to the experimental density of 2.624 g/cm^3. The systems

Table 1 Shell model interatomic potential: analytic functions and parameters [22]

	A (eV)	ρ (Å)	C (eV Å^6)
Buckingham $Ae^{-r/\rho} - C/r^6$			
O_s–O_s	22,764.30	0.1490	27.88
Si–O_s	1,283.91	0.32052	10.661580
Ca–O_s	2,152.3566	0.309227	0.09944
Al–O_s	1,460.3000	0.29912	0.0000000
	k_b (eV rad^{-2})	θ_0 (deg)	ρ (Å)
Three-body potential $\frac{1}{2}k_b(\theta - \theta_0)^2\exp(-[r_{12}/\rho + r_{13}/\rho])$			
O–Si–O	100.0	109.47	1.0
O–Al–O	100.0	109.47	1.0
		k_s (eV Å^{-2})	Y (e)
Core–shell potential $1/2k_sr^2$			
O_c–O_s		74.92	−2.8482

were heated and hold at 3,200 K for 100 ps in the NVT ensemble ensuring a suitable melting of the samples. The liquids were then cooled to 300 K at a nominal cooling rate of −5 K/ps. The resulting glass structures were subjected to a final NVT trajectory of 200 ps [2].

2.2 NMR parameters calculation

NMR calculations were carried out with the CASTEP [25] density functional theory (DFT) code using the GIPAW [15] algorithm, which allows the reconstruction of the all electrons wave function in the presence of a magnetic field. The generalized gradient approximation (GGA) PBE [26] functional was employed, and the core–valence interactions were described by ultrasoft pseudopotentials generated on the fly [27]. For ^{17}O, the 2s and 2p orbitals were considered as valence states with a core radius of 1.3 Å; for ^{29}Si and ^{27}Al, a core radius of 1.8 Å was used with 3s and 3p valence orbitals, while for ^{43}Ca, a core radius of 2.0 Å was used with 3s, 3p and 4s valence states.

For the PAW and GIPAW calculations, we used two projectors in each s and p angular momentum channel for O, and in the s, p and d channel for Si, Al and Ca.

It is well known that in the PBE approximation, the energy of Ca 3d orbital is too low and the hybridization with O 2p orbitals is overestimated [17]. As a consequence, the ^{17}O chemical shifts computed with PBE are affected by very large errors (up to 124 ppm) for O sites close to Ca atoms. To overcome this problem, a modified Ca pseudopotential with shifted 3d orbitals of 3.2 eV has been used as proposed by Profeta et al. [17].

Before computing the NMR parameters, constant pressure geometry optimizations of the classical generated models were performed at the Γ point [28]. Wave functions were expanded in plane waves with the kinetic energy cutoff of 700 eV, this has been demonstrated to be long enough to reach energy and NMR chemical shift converged values [10, 29].

The shielding tensor $(\overleftrightarrow{\sigma})$ is defined as the proportionality factor between the induced and the externally applied magnetic fields at the positions of the nuclei:

$$\overleftrightarrow{\sigma}(R) = \vec{B}_{\text{ind}}(R)/\vec{B}, \tag{4}$$

where $\vec{B}_{\text{ind}}(R)$ is the inhomogeneous magnetic field induced by the external field $\vec{B}$ and it can be calculated according to the Biot-Savart law:

$$\vec{B}_{\text{ind}}(\vec{r}) = \frac{\mu_0}{4\pi}\int d^3\vec{r}' \frac{\vec{r}' - \vec{r}}{\left|\vec{r}' - \vec{r}\right|^3} \times \vec{j}\left(\vec{r}'\right), \tag{5}$$

where the induced current can be obtained from the first-order perturbation theory [15].

Then, the isotropic chemical shift, δ_{iso}, can be obtained from the isotropic chemical shielding, σ_{iso}:

$$\sigma_{\text{iso}} = 1/3 Tr\{\overleftrightarrow{\sigma}\} \tag{6}$$

$$\delta_{\text{iso}} = -(\sigma_{\text{iso}} - \sigma_{\text{ref}}), \tag{7}$$

where σ_{ref} is a reference isotropic shielding. From the principal components of the symmetric part of the chemical shift tensor, the magnitude, δ_{CSA}, and asymmetry, η_{CSA}, of the chemical shift anisotropy (CSA) can be calculated:

$$\delta_{\text{CSA}} = \delta_{ZZ} - \delta_{\text{iso}} \tag{8}$$

$$\eta_{\text{CSA}} = \frac{(\delta_{YY} - \delta_{XX})}{(\delta_{ZZ} - \delta_{\text{iso}})}, \tag{9}$$

where δ_{ii} are the principal components of the symmetric chemical shift tensor such that $|\delta_{ZZ} - \delta_{\text{iso}}| \geq |\delta_{YY} - \delta_{\text{iso}}| \geq |\delta_{XX} - \delta_{\text{iso}}|$.

Nuclei with a spin >½ have quadrupolar parameters related to the traceless electric field gradient tensor $\vec{V}(\vec{r})$:

$$V_{\alpha\beta}(\vec{r}) = \frac{\partial E_\alpha(\vec{r})}{\partial r_\beta} - \frac{1}{3}\delta_{\alpha\beta}\sum_\gamma \frac{\partial E_\gamma(\vec{r})}{\partial r_\gamma}, \quad (10)$$

where α, β and γ denote the Cartesian coordinates x, y, and z, and $E_\alpha(\vec{r})$ is the local electric field at the position $(\vec{r})$. If the eigenvalues of the EFG tensor are labeled V_{xx}, V_{yy}, V_{zz} so that $|V_{zz}| > |V_{yy}| > |V_{xx}|$, then one can define the quadrupolar coupling constant as

$$C_Q = \frac{eQV_{zz}^{PAF}}{h} \quad (11)$$

And the asymmetry parameter as:

$$\eta_Q = \frac{V_{xx} - V_{yy}}{V_{zz}} \quad (12)$$

In this work, the δ_{iso} of ^{27}Al, ^{17}O and ^{43}Ca were evaluated using the shielding references (σ_{ref}) of 555.4, 260.5 and 1,134.1 ppm obtained by α-corundum, α-cristobalite and CaO, respectively, and the experimentally determined quadrupolar moment, eQ, of 146.6, 25.58 and 40.9 mB was used for ^{27}Al, ^{17}O and ^{43}Ca atoms [30].

The simulation of the solid-state MAS and 3QMAS NMR spectra from the CASTEP outputs have been carried out by means of the software fpNMR [10, 31]. For each atomic site i, the NMR spectrum of interest, say $I_i(\vec{v})$, is calculated and then co-added to yield the final NMR spectra $I(\vec{v}) = \sum_i I_i(\vec{v})$. The software allows the summation to be restricted to a given chemical speciation of the considered atom and to merge the spectra of several structural models to increase the statistical data.

Finally, it is worth noting that the aforementioned approach is a common procedure in ab initio calculations of glasses and enables only short-range relaxations at the ab initio level, whereas the medium-range structure, such as the connectivity of the glass-forming sites, is "frozen" to the initial configuration obtained by classical MD.

However, several papers have demonstrated that the present approach is adequate to study the local structure, such as the coordination environment of ions in bioactive glasses [32], and important vibrational features [33–35] and NMR parameters [11, 36].

3 Results and discussion

The structure of alkali or alkaline earth aluminosilicate glasses has since long been understood in terms of a three-dimensional connected structure of $[SiO_4]^{4-}$ and $[AlO_4]^{5-}$ tetrahedra linked at the corners by bridging oxygen (BO) atoms. In this picture, a fully connected network structure can be maintained if the charge deficit created by the substitution of Si^{4+} with Al^{3+} is compensated by 'charge balancing' cations such as Na^+ or Ca^{2+} located close to aluminum.

According to this model, the glass reaches maximum polymerization for a total compensation of charges by the cations, for instance, for calcium the system results fully polymerized at a ratio $[CaO]/[Al_2O_3] = 1$.

Any excess of Ca^{2+} will acquire non-bridging oxygens (NBO) between themselves and a tetrahedral cation (Al, Si), thus interrupting the network connectivity.

However, recent experiments have shown that the compensated continuous random network model is not entirely correct for some aluminosilicate compositions. In particular, both precise measurements of the viscosity of Na- and Ca-aluminosilicate liquids [37] and high-resolution ^{17}O MQMAS experiments [38] indicate that the network in aluminosilicate glasses with a tectosilicate composition (that is, where the ratio $[CaO]/[Al_2O_3]$ is equal to one) is not fully polymerized and that NBO exist in the system. At the same time, to preserve the total number of Al–O and Si–O bonds, the presence of NBO is compensated by oxygen triclusters, also called three bridging oxygens (TBO). That is, oxygen bounded to three Al and/or Si atoms which are fourfold-coordinated.

To elucidate better the local environment around aluminum ions and corroborate recent experimental evidences on the oxygen speciation, the theoretical ^{27}Al and ^{17}O MAS and 3Q-MAS spectra of the structural models generated by classical molecular dynamics simulations will be analyzed in details in the following paragraphs.

3.1 ^{27}Al NMR spectroscopy

Figure 1a shows the ^{27}Al MAS NMR spectrum of the CAS glass obtained as the summation of the NMR spectra of the two structural models containing 250 atoms each. Then, the merged spectrum has been normalized to be comparable to the experimental one which has been digitalized from Ref. [39] and reported in the bottom panel of the figure. Both the experimental and the simulated spectra were collected/simulated at a magnetic field of 11.7 T and at a spinning frequency of 14 kHz.

The simulated ^{27}Al MAS spectrum is in fairly agreement with the experimental one, which shows a chemical shift of about 50 ppm confirming that all the aluminum atoms are found in tetrahedral configuration.

Among the 60 Al atoms present in the two structural models studied only one is fivefold coordinated with $\delta_{\text{iso}} = 10.7$ ppm, $\delta_{\text{CSA}} = -15.6$ ppm, $\eta_{\text{CSA}} = 0.45$,

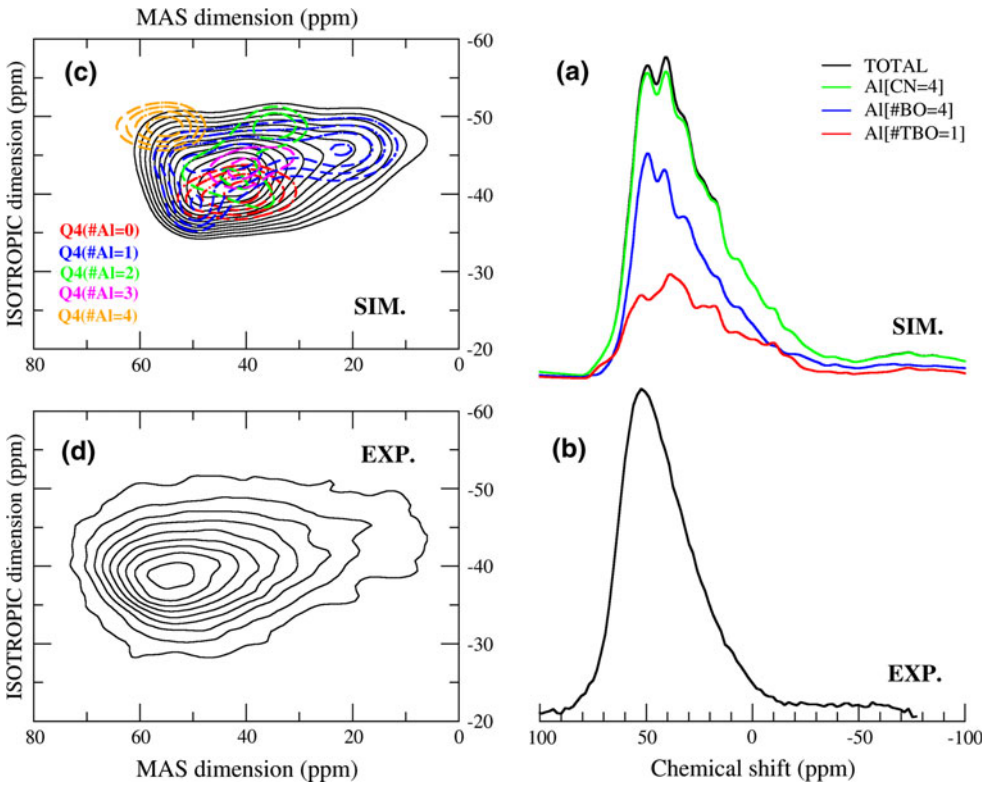

Fig. 1 **a** Simulated and **b** experimental ^{27}Al MAS spectra of the CAS glass. The *green line* represents the spectrum of fourfold-coordinated Al ions without NBO connected with them; the *blue line* represents the spectrum of Al ions connected to 4 BO, while the *red line* represents the spectrum of Al ions connected to 1 TBO and 3 BO. **c** Simulated and **d** experimental ^{27}Al 3Q-MAS spectra of the CAS glass. The signals generated by Al ions with 0, 1, 2, 3 and 4 Al ions in the second coordination sphere are also reported in the theoretical spectrum

$C_Q = 6.5$ MHz and $\eta_Q = 0.51$ and one is a Q^3 species with $\delta_{iso} = 62.9$ ppm. Therefore, penta-coordinated Al atoms, if present in the experimental structure of the glass, should be detectable as a shoulder in the tail of the spectrum. Conversely, the signals coming from Q^3 species could not be easily extracted from the experimental spectra since they range in the same region as for Q^4 species.

Hence, the structure of the glass is governed by aluminum atoms surrounded by 4 oxygens of the BO or TBO type, the spectrum of which is represented as the green line in Fig. 1a.

Despite the good agreement between the simulated and the experimental spectra, some inconsistencies are present. In particular, the latter is narrower than the former probably because of a distorted tetrahedral arrangement of the aluminum atoms in the modeled structure. In fact, although both the mean O–Si–O and O–Al–O bond angles are located at the same value of 109°, the standard deviation is greater for Al (9.9°) than for Si (4.7°). These findings are in nice agreement with previous Car-Parrinello MD simulations carried out by Benoit et al. [40] on aluminosilicate glasses with a tectosilicate composition.

The second noticeable inconsistency in the simulated ^{27}Al MAS spectrum regards the presence of a second peak at around 40 ppm, which is imputable to Al atoms connected to 1 TBO (reported as red line signal in Fig. 1a) besides the signal of Al atoms connected to only 4 BO atoms which is located at around 50 ppm.

Indeed, in the models obtained 40% of the Al atoms have at least 1 TBO in the first coordination sphere, a value that is probably too high. The presence of TBO in the first coordination sphere leads to a non-ideal tetrahedral arrangement because of the reduction of the O–Al–O angles and thus to a greater standard deviation for this angle and a broader ^{27}Al MAS NMR spectrum.

The high amount of TBO found in our models is in agreement with Car-Parrinello MD simulations [40], suggesting that their presence might be a consequence of the small system sizes and the very fast quenching rate that we are forced to use in our computational investigations [2, 41] but inaccuracies due to the empirical force field employed cannot be excluded.

The mean structural features (bond lengths and bond angles) and NMR parameters (isotropic chemical shift, chemical shift anisotropy and quadrupolar coupling constants) of Al ions with 1 or 2 TBO in the first coordination sphere are reported in Table 2. Interestingly, while the isotropic chemical shift does not seem to be affected by the presence of TBO since it lies at around 60–61 ppm, a value close to the experimental value of 66 ppm reported by Angeli et al. [39], the quadrupolar coupling constant (C_Q) increases with the amount of TBO in the first coordination

Table 2 Structural features and computed NMR parameters of aluminum in the CAS glass

	Al	Al (Q^4)	Al (#TBO = 1)	Al (#TBO = 2)
# of atoms	60	58	22	2
Al–O (Å)	1.77 (0.07)	1.77 (0.02)	1.77 (0.04)	1.80
Al–NBO	1.75	–	–	–
Al–BO	1.76 (0.03)	1.76 (0.02)	1.76 (0.04)	1.74
Al–TBO	1.83 (0.05)	1.82 (0.05)	1.82 (0.05)	1.86
O–Al–O (°)	109.2 (7.8)	109.3 (9.0)	109.1 (11.1)	109.4
Al–O–T (°)	132.3 (16.5)	132.4 (16.3)	128.8 (17.9)	124.6
δ_{iso} (ppm)	61.1 (10.3)	61.9 (8.0)	60.4 (13.2)	61.0
δ_{CSA} (ppm)	−8.8 (29.2)	−9.1 (29.6)	−7.4 (30.3)	−19.1
η_{CSA}	0.62 (0.22)	0.63 (0.22)	0.57 (0.24)	0.59
C_Q (MHz)	9.49 (2.8)	9.58 (2.8)	9.86 (3.0)	11.86
η_Q	0.64 (0.23)	0.64 (0.23)	0.61 (0.20)	0.80
P_Q (MHz)	10.14 (9.9)	10.24 (9.9)	10.48 (3.0)	13.0

Standard deviations are reported in parenthesis

sphere from 9.58 to 11.86 MHz for Al atoms with 0 to 2 TBO, respectively.

Regarding the structural features connected to the short-range order of Al ions, the DFT-optimized structural models provide a mean Al–O bond length of 1.77 Å, which is in very good agreement with experimental distances measured in aluminosilicate glasses and crystalline analogous of different compositions [42–46].

The Al–O bond increases with the number of TBO connected to the central Al atom, while the mean Al–O–T angle decreases from 132.4° to 124.6° for Al atoms surrounded by 0 and 2 TBO, respectively.

As expected, the Al–NBO bond distance (1.75 Å) is shorter than the Al–BO one (1.76 Å) which in turn is shorter than the Al–TBO bond distance (1.83 Å).

Further precious information on the medium-range structure and the Al/Si ratio in aluminosilicate glasses can be gained by analyzing the ^{27}Al 3QMAS spectrum as reported in Fig. 1c.

The simulated ^{27}Al 3QMAS spectrum is shown in the upper panel of the figure together with the contributions of tetrahedral Al ions surrounded by $n = 0,\ldots,4$ Al atoms in the second sphere. These units are denoted with the following symbolism [Q4(#Al = n)], while the mean structural and NMR parameters of the different speciation of Al atoms are reported in Table 3.

The detailed analysis of the second coordination sphere of Al ions shows that the medium-range order of the studied glass is governed by Q^4(4Si) (27%), Q^4(3Si,1Al) (40%) and Q^4(2Si,2Al) (22%) units which are depicted in Fig. 2.

Table 3 shows that the isotropic chemical shift increases with the amount of Al ions in the second coordination sphere from 58.7 ppm (for Q^4(4Si)) to 72.1 ppm (for Q^4(4Al)) as well as the quadrupolar coupling constant C_Q

Table 3 Mean structural features and computed NMR parameters of the Q^4 species of aluminum depending on the network former present in the second coordination sphere

	Q^4(4Si)	Q^4(3Si,1Al)	Q^4(2Si,2Al)	Q^4(1Si,3Al)	Q^4(4Al)
# of atoms	16	24	13	4	3
Al–O (Å)	1.77 (0.01)	1.77 (0.02)	1.78 (0.05)	1.78 (0.03)	1.76 (0.02)
Al–BO	1.76 (0.01)	1.76 (0.02)	1.76 (0.05)	1.77 (0.02)	1.75 (0.01)
Al–TBO	1.91	1.85 (0.06)	1.81 (0.08)	1.82 (0.07)	1.78 (0.02)
O–Al–O (°)	109.4 (8.3)	109.2 (9.5)	108.9 (12.8)	109.0 (8.8)	109.4 (7.5)
Al–O–T (°)	136.3 (14.7)	134.3 (17.8)	129.9 (14.3)	122.6 (15.9)	124.6 (11.3)
δ_{iso} (ppm)	58.7 (5.8)	61.0 (8.9)	60.7 (16.6)	64.4 (1.5)	72.1 (6.6)
δ_{CSA} (ppm)	−2.5 (24.0)	−9.8 (32.0)	−13.5 (31.0)	−22.0 (28.0)	3.5 (24.7)
η_{CSA}	0.67 (0.14)	0.65 (0.22)	0.51 (0.14)	0.56 (0.16)	0.74 (0.24)
C_Q (MHz)	8.61 (2.6)	10.05 (2.9)	10.17 (3.4)	8.71 (1.6)	7.7 (1.4)
η_Q	0.62 (0.12)	0.63 (0.23)	0.60 (0.18)	0.76 (0.19)	0.77 (0.14)
P_Q (MHz)	9.18 (2.6)	10.73 (3.0)	10.80 (3.5)	9.55 (3.5)	8.46 (1.4)

Standard deviations are reported in parenthesis

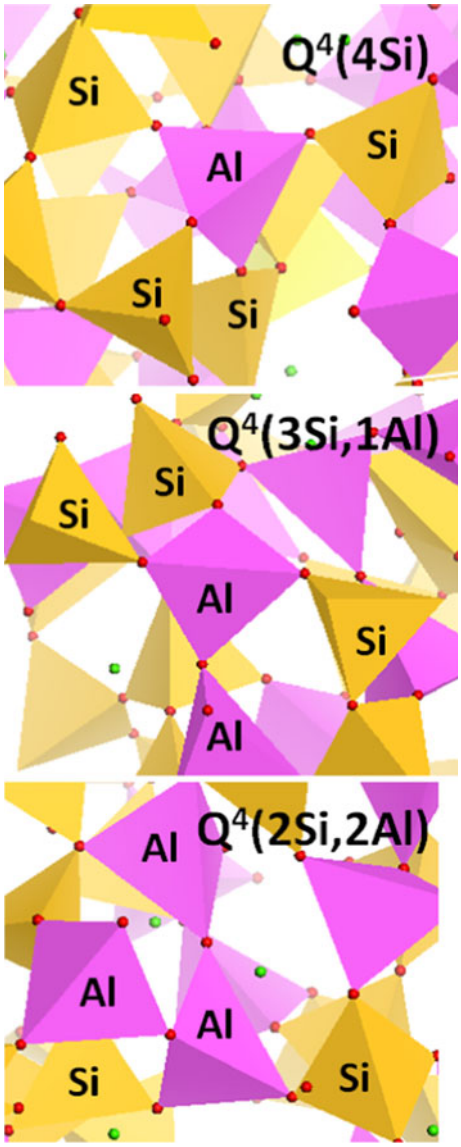

Fig. 2 Local environment (medium-range order) of each AlO_4 tetrahedron found in the CAS glass. *Violet tetrahedral* represents AlO_4 units, while the *yellow* ones represent SiO_4 units

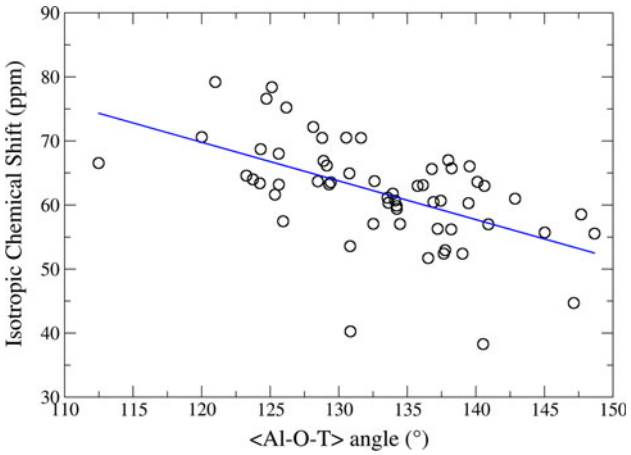

Fig. 3 Simulated ^{27}Al isotropic chemical shift as a function of the mean <Al–O–T> angle

which increases from 8.6 MHz (for Q^4(4Si)) to 10.2 MHz (for Q^4(2Si,2Al).

The presence of Al ions in the surrounding of AlO_4 units gives rise to a distortion in the tetrahedra as highlighted by the anisotropic chemical shielding (δ_{CSA}) whose absolute value increases from 2.5 ppm for Q^4(4Si) to 22 ppm Q^4(1Si,3Al) and by the standard deviation of the O–Al–O bond angle which increases from 8.8° to 12.5° for Q^4(4Si) and Q^4(2Si,2Al), respectively.

Another important structural parameter that is usually found to affect the ^{27}Al isotropic chemical shift is the average Al–O–T bond angle, where T is the tetrahedral atom Si or Al [47]. In Fig. 3, the ^{27}Al δ_{iso} is plotted against the mean <Al–O–T> angle for the CAS glass studied. Linear regression analysis of the data as $\delta_{iso} = a \cdot \langle Al - O - T \rangle + b$ points yields a slope of −0.60 and intercept of 142.27° with a poor correlation coefficient ($R^2 = 0.303$).

As it has been underlined in a recent paper by some of us [10], the presence of Ca ions in the glass structure yields worst correlations with respect to that obtained when the modifier is an alkaline ion such as Na or Li for which the linear fit yields R^2 values in the range 0.7–0.9 [36]. However, notwithstanding the poor correlation coefficient, it can be noticed that by increasing Al–O–T bond angle, the ^{27}Al chemical shift decreases, thus confirming the results of previous experimental and theoretical studies regarding the relationship between δ_{iso} and Al–O–T bond angle [48, 49].

The rationale behind the correlation between the shielding properties of Al atoms and the values of the Al–O–T angle has been unveiled by Liu et al. [47] in their ab initio NMR shielding calculations, natural bonding orbital analysis and natural chemical shielding analysis performed on model clusters with different Al–O–T angles. Based on Hartree–Fock calculations, they demonstrated that the opening of the Al–O–T bond angle leads to a slight increase in the population of the Al–O and Si–O bond orbital electrons and a dramatic change in the bond orbital shapes and hybridization (with an increase in the s character and a decrease in bond bending). Moreover, the movement of one lone pair on the oxygen toward Al or Si contributes to the shielding of both Al and Si.

3.2 ^{17}O NMR spectroscopy

Oxygen-17 NMR is an ideal method for the direct investigation of whether NBO and TBO are indeed present in aluminum silicate glasses in which the $[CaO]/[Al_2O_3]$ ratio is equal to one. In a pioneering work, Stebbins and Xue

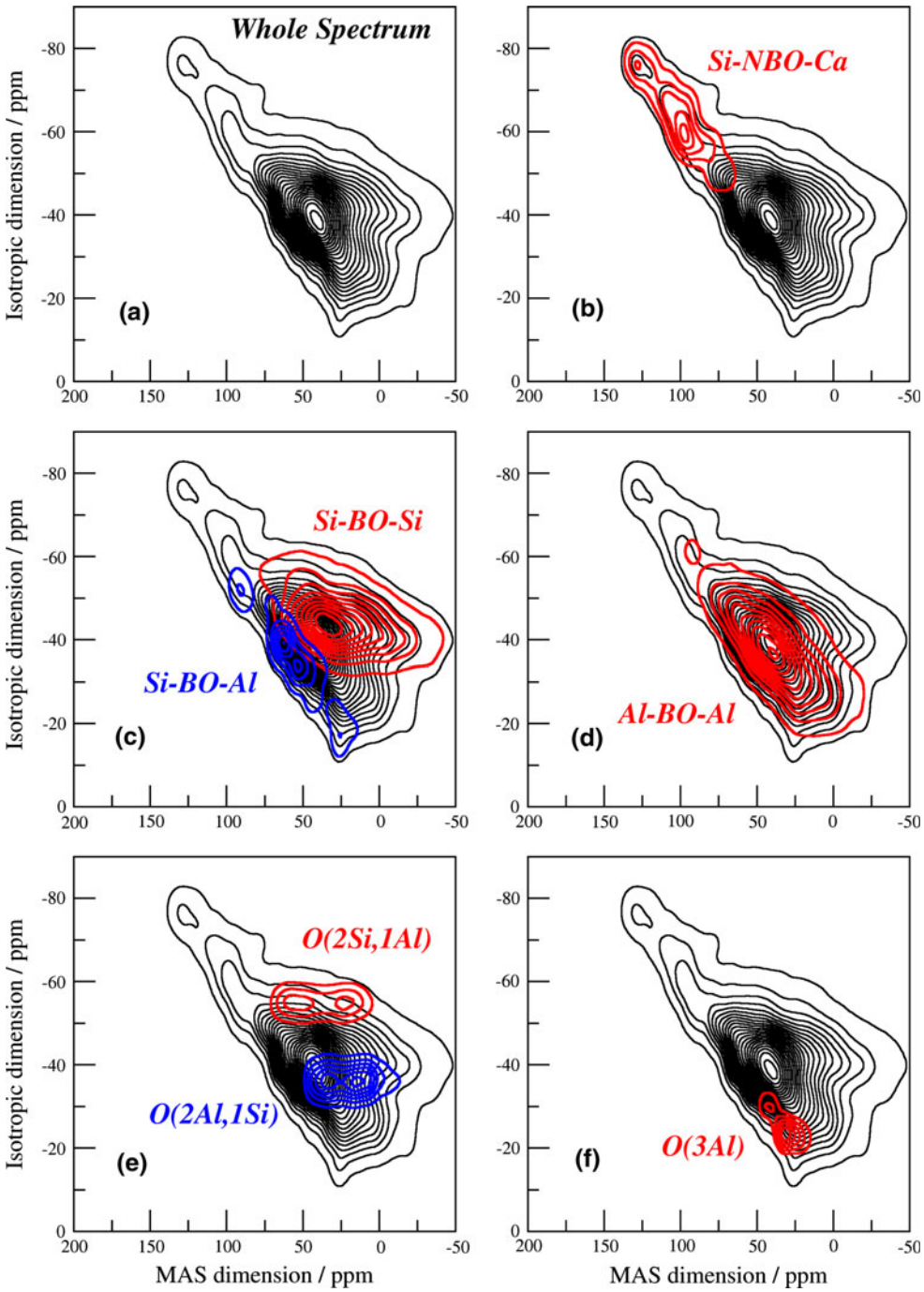

Fig. 4 **a** Simulated oxygen-17 3QMAS NMR spectrum at 11.75 T of the CAS glass. The signals of the different oxygen speciation are also superimposed in the panels from **b** to **f**

[38] found that the 3QMAS spectrum of the $CaAl_2Si_2O_8$ was composed essentially by four peaks denoted as A, B, C and D. Peak A was associated with NBO atoms whose isotropic chemical shift (δ_{iso}) and quadrupolar coupling constant (C_Q) were calculated to be 113 ± 2 ppm and 2.9 ± 0.2 MHz. The peak B, assigned to Si–O–Al bonds, was the main one with $\delta_{iso} = 61$ ppm and $C_Q = 3.5$ MHz, while peak C (50 ppm, 5.5 MHz) was associated with Si–O–Si bonds. Finally, they detected a small peak, called D, with $\delta_{iso} = 20$ ppm and $C_Q = 2.3$ MHz, which was supposed to be the signal arising from OAl_3 or OAl_2Si triclusters, in which Al remains in four-coordination.

To help in the interpretation of the experimental spectrum, the simulated ^{17}O 3QMAS NMR spectrum is reported in Fig. 4, together with the spectra generated for the different oxygen speciation present in our models (see panels from b to f).

It is worth to highlight here that albeit the glass studied in this paper has a different composition with respect to that investigated by Stebbins et al. [38] both are

Table 4 Computed NMR parameters and population of oxygen speciation

	δ_{iso} (ppm)	C_Q (MHz)	η_Q	Population (%)
OSi_2	61.0 (10.9)	5.18 (0.54)	0.41 (0.26)	28.5
OAl_2	62.6 (17.7)	2.26 (0.43)	0.62 (0.25)	6.4
OSiAl	58.2 (15.6)	3.80 (0.46)	0.53 (0.27)	55.8
OSi	110.9 (16.1)	2.85 (0.45)	0.44 (0.25)	5.4
OAl	159.5	1.18	0.45	0.3
OSi_2Al	77.4 (1.1)	5.53 (0.19)	0.32 (0.19)	0.6
$OSiAl_2$	50.1 (2.8)	4.66 (0.32)	0.49 (0.27)	1.1
OAl_3	41.9 (11.9)	3.15 (0.71)	0.38 (0.21)	1.9

Standard deviations are reported in parenthesis

tectosilicate glasses with a unitary $[CaO]/[Al_2O_3]$ ratio and thus the same type of structural units (NBO and TBO) is present in the structure. Although the site populations might be slightly different leading to differences in the shape of the NMR spectrum, the peak positions of these important structural features are only slightly affected by the glass composition and the comparison of the ^{17}O NMR spectra between the two glasses is justified.

The computed mean NMR parameters (δ_{iso}, C_Q, η_Q) and the population of the T-NBO, T–BO–T and TBO structural units are reported in Table 4. Hopefully, these values might be used to guide the fitting of the experimental ^{17}O 3QMAS spectrum for resolving and quantifying better the different structural units present in the glass in future works.

It is worth noticing that both the simulated spectrum and the NMR parameters of the different species are in good agreement with those reported by Stebbins and Xue [38].

In particular, the structural model obtained in this work contains 5.4% of NBO connected to Si atoms with $\delta_{iso} = 111$ ppm and $C_Q = 2.85$ MHz and 0.3% of NBO bounded to Al whose NMR parameters (159 ppm, 1.2 MHz) are very different with respect to the ones of NBO–Si units. Therefore, if present in the experimental structure, they should be easily detectable by both ^{17}O MAS and 3QMAS NMR experiments; however, so far, no experimental evidence has been found regarding the presence of these structural units in glasses with a tectosilicate composition as that studied in this work.

Among the bridging oxygens, 55.4% of them form Si–O–Al units (58.2 ppm, 3.8 MHz), 28.5% are present as Si–O–Si units (61 ppm, 5.2 MHz) and 6.4% as Al–O–Al units (62.6 ppm, 2.3 MHz). These units have similar isotropic chemical shifts but different C_Q values, which make the Si–O–Al and Si–O–Si units quite distinguishable in the bi-dimensional spectrum. Instead, the Al–O–Al peak that accompanies Al/Si disorder in the glass is hidden by the Si–O–Al and Si–O–Si peaks (see Fig. 4c, d).

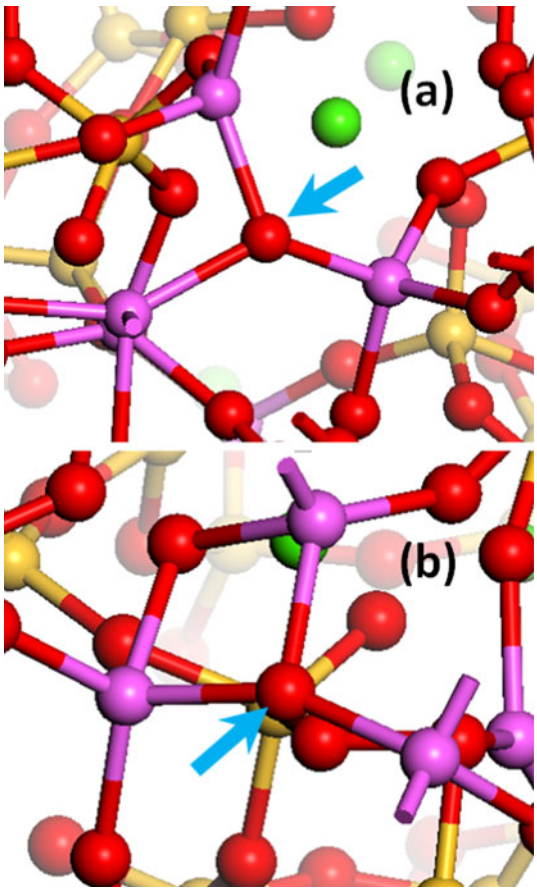

Fig. 5 Local geometry of OAl_3 sites found in the simulated glass. The oxygen tricluster is highlighted by a *light blue arrow*. **a** Al atoms (*violet spheres*) contribute to the formation of large rings. **b** Al atoms form a 2-membered Al_2O_2 ring

As already reported in previous Car-Parrinello molecular dynamics simulations of CAS glasses with similar compositions [40], also in our structural models, the excess number of NBO is compensated by the existence of OAl_2Si (1.1%), $OAlSi_2$ (0.6%) and OAl_3 (1.9%) tricluster oxygens whose contributions to the 3QMAS spectrum are shown in Fig. 4e, f.

Figure 4e and Table 4 clearly reveal that the NMR parameters of the OAl_2Si (50.1 ppm, 4.66 MHz) and $OAlSi_2$ (77.4 ppm, 5.53 MHz) are in the same range covered by the Si–O–Si and Si–O–Al sites, and since these triclusters are present in the glass in very small quantities, it is very unlikely that 3QMAS NMR could detect them. Conversely, the NMR parameters of the OAl_3 triclusters are close to the edge of the main Si–O–Al peak and their position (see Fig. 4f) is in nice agreement with the peak D observed by Stebbins et al. [38].

The five OAl_3 sites found in the simulated glass structure are present in two structural motifs shown in Fig. 5; in particular, in one of these OAl_3 sites, two of the Al atoms

form a 2-membered Al_2O_2 ring (Fig. 5b), whereas in the other four sites, Al is part of larger rings (Fig. 5a).

A punctual analysis of the NMR parameters associated with these sites shows that, whereas for the most populated motif the C_Q value ranges between 2.6 and 3.5 MHz, the oxygen tricluster in the 2-membered Al_2O_2 ring shows the small value of $C_Q = 2.4$ MHz consistent with the experimental observations of Stebbins and Xue [38]. Therefore, the results obtained seem to support the experimentalist' assignments of the D peak in the 3QMAS spectra to O triclusters with a local geometry similar to that depicted in Fig. 5b, although it must be noted that the calculated isotropic chemical shift of 40 ppm is much greater than that proposed by Stebbins and Xue [38].

4 Conclusions

In this work, a calcium aluminosilicate glass with a 'tectosilicate' composition has been generated by core–shell classical molecular dynamics simulations and its structure has been compared with NMR experiments by simulating the ^{27}Al and ^{17}O MAS and 3QMAS NMR spectra.

The structural model obtained contains an excess of NBO, which are compensated by the presence of O triclusters connected to three AlO_4 or SiO_4 tetrahedra.

The simulated ^{27}Al NMR spectra are in fairly agreement with the experimental ones and they confirm that all the aluminum atoms are found in tetrahedral configuration. However, it seems that the structural model obtained in this paper overestimates the amount of Al atoms (40%) connected to at least 1 TBO in their first coordination sphere. The presence of TBO leads to a non-ideal tetrahedral geometry around Al and increases the value of the quadrupolar coupling constant C_Q. As a consequence, the MAS NMR spectra result broader with the appearance of a double peak not detected experimentally.

The detailed analysis of the second coordination sphere of Al ions shows that the medium-range order of the studied glass is governed by Q^4(4Si) (27%), Q^4(3Si,1Al) (40%) and Q^4(2Si2Al) (22%) species. Both the isotropic chemical shift and C_Q increase with the amount of Al ions in the second coordination sphere.

The analysis of the oxygen site populations and of the ^{17}O NMR spectra support the experimentalist' assignments of the peaks in the 3QMAS spectra, reported by Stebbins.

In particular, the structural model obtained in this work contains 5.4% of NBO connected to Si atoms, 55.4% of the oxygens form Si–O–Al units, 28.5% are present as Si–O–Si units, 6.4% are present as Al–O–Al units and 3.6% as O triclusters. Among the O triclusters, only those in the 2-membered Al_2O_2 rings shows the small value of $C_Q = 2.4$ MHz consistent with the experimental observations of Stebbins and Xue.

Acknowledgments The authors thank the Italian Ministry of University and Research for funding (Project COFIN2008, prot. 2008J9RNB3 "Integrazione Temporale per l'Evoluzione Molecolare"). A. P. thanks Dr. Thibault Charpentier of the CEA, IRAMIS, Service Interdisciplinaire sur les Systémes Moléculaires et Matériaux (Paris, France) for fruitful discussions.

References

1. Massiot D, Fayon F, Montouillout V, Pellerin N, Hiet J, Roiland C, Florian P, Coutures J-P, Cormier L, Neuville DR (2008) J Non-Cryst Solids 354(2–9):249–254
2. Pedone A (2009) J Phys Chem C 113:20773–20784
3. Stebbins JF (1995) In: Stebbins JF, McMillan PF, Dingwell DB (eds) Reviews in mineralogy, vol 32. MSA, Washington DC, p 191
4. Dupree E, Pettifer RF (1984) Nature (London) 308:523
5. Linati L, Lusvardi G, Malavasi G, Menabue L, Menziani MC, Mustarelli P, Pedone A, Segre U (2008) J Non-Cryst Solids 354:84–89
6. Maekawa H, Maekawa T, Kawamura K, Yokokawa T (1991) J Non-Cryst Solids 127:53
7. Voigt U, Lammert H, Eckert H, Heuer A (2005) Phys Rev B 72:64207
8. Frydman L, Harwod JS (1995) J Am Chem Soc 117:5367–5368
9. Medek A, Harwood S, Frydman L (1995) J Am Chem Soc 117:12779–12787
10. Pedone A, Charpentier T, Menziani MC (2010) Phys Chem Chem Phys 12:5064–6066
11. Pedone A, Charpentier T, Malavasi G, Menziani MC (2010) Chem Mater 22:5644–5652
12. Charpentier T, Ispas S, Profeta M, Mauri F, Pickard CJ (2004) J Phys Chem B 108:4147–4161
13. Pedone A, Pavone M, Menziani MC, Barone V (2008) J Chem Theory Comput 4:2130–2140
14. Tossell JA, Horbach J (2005) J Phys Chem B 109:1794–1797
15. Pickard CJ, Mauri F (2001) Phys Rev B 63:245101
16. Profeta M, Mauri F, Pickard CJ (2003) J Am Chem Soc 125:541–548
17. Profeta M, Benoit M, Mauri F, Pickard CJ (2004) J Am Chem Soc 126:12628–12635
18. Tielens F, Gervais C, Lambert JF, Mauri F, Costa D (2008) Chem Mater 20:3336–3344
19. Ferlat G, Charpentier T, Seitsonen AP, Takada A, Lazzeri M, Cormier L, Calas G, Mauri F (2008) Phys Rev Lett 101:065504
20. Dick G, Overhauser AW (1958) Phys Rev 112:90
21. Pedone A, Corno M, Civalleri B, Malavasi G, Menziani MC, Segre U, Ugliengo P (2007) J Mater Chem 17:2061–2068
22. Tilocca A, de Leeuw NH, Cormack AN (2006) Phys Rev B 73:104209
23. Smith W, Forester TR (1996) J Mol Graph 14:136
24. Pedone A, Malavasi G, Menziani MC (2009) J Phys Chem C 113:15723–15730
25. Segall MD, Lindan PJD, Probert MJ, Pickard CJ, Hasnip PJ, Clarck SJ, Payne MC (2002) J Phys: Condens Matter 14:2717
26. Perdew JP, Burke K, Ernzerhof M (1996) Phys Rev Lett 77:3865
27. Yates JR, Pickard CJ, Mauri F (2007) Phys Rev B 76:024401
28. Monkhorst H, Pack JD (1976) Phys Rev B 13:5188
29. Choi M, Matsunaga K, Oba F, Tanaka I (2009) J Phys Chem C 113:3869–3873

30. Pyykkò P (2001) Mol Phys 99:1617
31. Charpentier T, Kroll P, Mauri F (2009) J Phys Chem C 113:7917–7929
32. Malavasi G, Menziani MC, Pedone A, Civalleri B, Corno M, Ugliengo P (2007) Theor Chem Acc 117:933–942
33. Tilocca A (2007) Phys Rev B 76:224202
34. Corno M, Pedone A, Dovesi R, Ugliengo P (2008) Chem Mater 20:56105621
35. Corno M, Pedone A (2009) Chem Phys Lett 476:218–222
36. Angeli F, Villain O, Schuller S, Ispas S, Charpentier T (2011) Geochim Cosmochim Acta 75:2453–2469
37. Toplis MJ, Dingwell DB (1996) Trans Am Geophys Un 77:F848
38. Stebbins JF, Xu Z (1997) Nature 390:60–62
39. Angeli F, Gaillard M, Jollivet P, Charpentier T (2007) Chem Phys Lett 440:324–328
40. Benoit M, Profeta M, Mauri F, Pickard CJ, Tuckerman ME (2005) J Phys Chem B 109:6052–6060
41. Pota M, Pedone A, Malavasi G, Durante C, Cocchi M, Menziani MC (2010) Comput Mater Sci 47:739
42. Brown GE, Gibbs GV, Ribbe PH (1969) Am Miner 54:1044
43. Taylor M, Brown GE (1979) Geochim Cosmochim Acta 43:61
44. Himmel B, Weigelt J, Gerber T, Nofz M (1991) J Non-Cryst Solids 136:27
45. Petrov V, Gerber T, Himmel B (1998) Phys Rev B 58:11982
46. Petrov V, Billinger SJL, Shastri SD, Himmel B (2000) Phys Rev Lett 85:3436
47. Liu Y, Nekvasil H, Tossell JA (2005) J Phys Chem A 109:3060–3066
48. Farnan I, Grandinetti PJ, Baltisberger JH, Stebbins JF, Werner U, Eastman MA, Pines A (1992) Nature 358:31
49. Tossell JA (2001) Rev Miner 42:435